ResearchGate

See discussions, stats, and author profiles for this publication at: https://www.researchgate.net/publication/334490385

AMPK and AKT protein kinases hierarchically phosphorylate the N-terminus of the FOXO1 transcription factor, modulating interactions with 14-3-3 proteins

Article *in* Journal of Biological Chemistry · July 2019

DOI: 10.1074/jbc.RA119.008649

CITATION
1

READS
41

9 authors, including:

Maria Saline
AstraZeneca
15 PUBLICATIONS **108** CITATIONS
SEE PROFILE

Madita Wolter
Eindhoven University of Technology
5 PUBLICATIONS **16** CITATIONS
SEE PROFILE

Anders Gunnarsson
AstraZeneca
43 PUBLICATIONS **548** CITATIONS
SEE PROFILE

Tomas Jacso
Nuevolution
11 PUBLICATIONS **172** CITATIONS
SEE PROFILE

Some of the authors of this publication are also working on these related projects:

outer membrane proteins View project

Single molecule microscopy View project

All content following this page was uploaded by Maria Saline on 09 January 2020.

The user has requested enhancement of the downloaded file.

JBC Papers in Press. Published on July 15, 2019 as Manuscript RA119.008649
The latest version is at http://www.jbc.org/cgi/doi/10.1074/jbc.RA119.008649

AMPK and AKT protein kinases hierarchically phosphorylate the N-terminus of the FOXO1 transcription factor, modulating interactions with 14-3-3 proteins

Maria Saline[1,3,5], Lukas Badertscher[1,5], Madita Wolter[2], Roxanne Lau[2], Anders Gunnarsson[1], Tomas Jacso[1,4], Tyrrell Norris[1], Christian Ottmann[2], Arjan Snijder[1,*]

[1]Discovery Biology, Discovery Sciences, R&D, AstraZeneca, Gothenburg, Sweden
[2]Laboratory of Chemical Biology, Department of Biomedical Engineering and Institute for Complex Molecular Systems, Eindhoven University of Technology, P.O. Box 513, 5600 MB, Eindhoven, The Netherlands

Running title: *Phosphorylation of S22 in FOXO1 attenuates 14-3-3 binding*

[3] Present address: Chalmers University of Technology, 412 96 Gothenburg, Sweden
[4] Present address: Nuevolution A/S, Rønnegade 8, 2100 Copenhagen, Denmark
[5] These authors contributed equally
* Corresponding author: Arjan Snijder, Discovery Biology, Discovery Sciences, R&D, AstraZeneca, Gothenburg, Sweden, arjan.snijder@astrazeneca.com, Tel +46317763691

Keywords: FOXO1 transcription factor, AMP-activated protein kinase (AMPK), AKT serine/threonine kinase (AKT, PKB), protein phosphorylation, post-translational modification, 14-3-3 interaction, 14-3-3 scaffolding protein, gene regulation, energy homeostasis, kinase signaling

Abstract

Forkhead box protein O1 (FOXO1) is a transcription factor involved in various cellular processes such as glucose metabolism, development, stress resistance, and tumor suppression. FOXO1´s transcriptional activity is controlled by different environmental cues through a myriad of post-translational modifications. In response to growth factors, the Serine/Threonine kinase AKT phosphorylates T24 and S256 in FOXO1 to stimulate binding of 14-3-3 proteins thereby causing FOXO1 inactivation. In contrast, low nutrients and energy levels induce FOXO1 activity. AMPK-activated protein kinase (AMPK), a master regulator of cellular energy homeostasis, partly mediates this effect through phosphorylation of S383 and T649 in FOXO1. In this study, we identified S22 as an additional AMPK phosphorylation site in FOXO1´s N-terminus with S22 phosphorylation preventing binding of 14-3-3 proteins. The crystal structure of a FOXO1 peptide in complex with 14-3-3 σ at 2.3 Å resolution revealed that this is a consequence of both steric hindrance and electrostatic repulsion. Furthermore, we found that AMPK-mediated S22 phosphorylation impairs T24 phosphorylation by AKT in a hierarchical manner. Thus, numerous mechanisms maintain FOXO1 activity via AMPK signaling: AMPK-mediated S22 phosphorylation directly and indirectly averts binding of 14-3-3 proteins, whereas phosphorylation of S383 and T649 complementary stimulates FOXO1 activity. Our results shed light on a mechanism that integrates inputs from both AMPK and AKT signaling pathways in a small motif to fine-tune FOXO1 transcriptional activity.

Introduction

The forkhead box O (FOXO) family of transcription factors are well conserved throughout evolution and they control the expression of a multitude of genes involved in various cellular processes. FOXO1 (FKHR), one of the family members, was shown to regulate cellular homeostasis, insulin and glucose metabolism, immune responses, cell cycle progression, apoptosis and senescence (1). Moreover, FOXO1-null mice are not able to complete embryonic development, confirming its essential role (2).

Downloaded from http://www.jbc.org/ by guest on January 9, 2020

The transcriptional activity of FOXO1 is tightly regulated through numerous post-translational modifications such as phosphorylation, methylation, acetylation, ubiquitination and glycosylation (reviewed in (3) & (4)). Multiple kinases are known to reduce FOXO1 activity via phosphorylation (e.g. AKT (5), CDK5 (6), PKA (7), CDK2 (8), CDK1 (9), DYRK1, GSK3 and CK1(10)). Of these, FOXO1 phosphorylation by the phosphoinositide 3-kinase/AKT (PI3K/AKT) pathway is extensively studied. In response to a range of extracellular stimuli like growth factors, insulin and cytokines, AKT phosphorylates T24, S256 and S319 in FOXO1 (11,12). This allows binding of 14-3-3 scaffolding proteins to FOXO1 and the consequent inhibition of transcriptional activity through export from the nucleus to the cytoplasm. 14-3-3 proteins are ubiquitously expressed in mammalian cells and they mainly regulate the function of binding partners by affecting their subcellular localization (13). Notably, a triple mutant of FOXO1 (T24A/S256A/S319A), which cannot be phosphorylated by AKT, is predominantly nuclear and constitutively active because interactions with 14-3-3 proteins are abolished (14).

In contrast, various kinases activate the transcriptional activity of FOXO1 (AMPK (15), MST1 (16), ERK and p38 (17)). AMP-activated protein kinase (AMPK) is a major regulator of cellular energy homeostasis and activated under conditions such as nutrient deprivation or oxidative stress (18-22). Yun et al. (15) showed that AMPK phosphorylates FOXO1 on residues S383 and T649, however, the molecular mechanism for increased FOXO1 activity upon phosphorylation of these residues remains elusive. Moreover, the authors suggested additional AMPK sites might exist that could further explain the regulation of the transcriptional activity of FOXO1 by AMPK.

In this work, we identified S22 in FOXO1 as an additional AMPK phosphorylation site. Structural and biophysical data elucidated that phosphorylation of S22 reduces binding of 14-3-3 proteins to FOXO1 through steric hindrance and electrostatic repulsion. At the same time, S22 phosphorylation indirectly prevented 14-3-3 binding by negatively regulating T24 phosphorylation by AKT. Interestingly, phosphorylation of T24 did not affect phosphorylation of S22 by AMPK to similar extents, suggesting a hierarchical crosstalk between both signaling pathways. Together, S22 phosphorylation both directly and indirectly abrogates complex formation with 14-3-3 proteins and thereby plays a central role for controlling the transcriptional activity of FOXO1.

Results

The N-terminal domain of FOXO1 is intrinsically disordered

The FOXO1 protein consists of three major functional domains: the Forkhead box domain (FHD) that is responsible for DNA binding, the C-terminal transcription activation domain (TAD) and the less characterized N-terminal domain (NTD). Moreover, the protein contains signals that mediate nuclear localization (NLS) and nuclear export (NES) (Fig. 1A). Whereas the FHD and TAD have been extensively studied, there is little known about the contribution of the NTD regarding transcriptional activity of FOXO1.

To better understand the structural features of the different domains of FOXO1, we first performed *in silico* predictions of the disorder tendency (23,24). This analysis suggested a folded FHD (154-244) that is flanked by predominantly disordered regions (disorder scores $\geq$ 0.5 Fig. 1A). Of note, crystal structures have been solved for the FOXO1 FHD (25,26) confirming a structured organization of this region. Next, we focused on the NTD and purified two recombinant proteins for structural examination using 2D NMR. One protein encompassed the full NTD (1-153) and the other a N-terminal region of the NTD (1-46), hereafter referred to as NTD and NTDΔ, respectively (Fig. 1B). The $^{1}H/^{15}N$ HSQC NMR spectra of NTDΔ (Fig. 1C) and the NTD (Fig. S1) both showed narrow dispersions of $^{1}H/^{15}N$ chemical shifts in the ^{1}H dimension (7.7-8.6 ppm), a characteristic of proteins lacking secondary structure elements. While backbone resonances of NTDΔ were fully assigned, individual assignments of amino acids in the entire NTD could not be obtained due to peak overlaps. Nevertheless, both spectra showed a

Downloaded from http://www.jbc.org/ by guest on January 9, 2020

high similarity in chemical shifts and linewidths, indicating an intrinsically disordered nature of the NTD. A secondary structure propensity (SSP) analysis (27) further confirmed a predominantly random coil conformation of NTDΔ based on the Cα and Cβ chemical shifts from the 3D $^{13}C/^{15}N$ HNCαCβ experiment (Fig. S2). Yet, residues 21-25 and 35-40 had positive average SSP scores, 0.19 and 0.08 respectively, suggesting a weak partial α-helical propensity of those regions.

The NTD retains unstructured properties upon T24 phosphorylation by AKT

The NTD of FOXO1 contains one of the two 14-3-3 binding motifs (amino acids 19-26) and phosphorylation of T24 by AKT is required to mediate interactions with 14-3-3 proteins. Interestingly, residues 21-25 showed a weak α-helical propensity (Fig. S2) and therefore, we hypothesized that phosphorylation of T24 might induce structural changes that could influence 14-3-3 binding.

To measure phosphorylation of T24 in time-resolved 2D $^{1}H/^{15}N$ HMQC NMR experiments, either NTDΔ or the full NTD were incubated with purified AKT. Over the course of 3 h, a single chemical shift appeared at 8.95/119.89 ($^{1}H/^{15}N$) ppm (Fig. 2A, Fig. S3A), a region typical for phosphorylated residues (28). Simultaneously, two chemical shifts assigned to T24 gradually disappeared from 7.97/116.45 ($^{1}H/^{15}N$) and 8.13/116.82 ($^{1}H/^{15}N$) ppm, highlighting a strong phosphorylation of T24 by AKT, as expected. The appearance of two distinct individual chemical shifts might be caused by specific *cis* and *trans* conformations of the flanking proline residue as observed with other intrinsically disordered proteins (IDPs) (29). NTDΔ contains 10 prolines and the presence of 15 Hα/N peaks in a $^{15}N/^{13}C$ Hα(Cα)N NMR spectra revealed that five prolines occur in both cis and trans conformations (Fig. S4). Apart from the changes in chemical shifts for T24, only minor differences were detected for residues in proximity to the phosphorylation site: L17/27, R19/29, R21, S22, C23 and Y25.

Finally, the SSP scores for both the unphosphorylated and T24 phosphorylated NTDΔ were comparable (Fig. S2). This suggested that T24 phosphorylation by AKT does not influence the local structural organization of the NTD.

AMPK phosphorylates S22 in the NTD

AMPK was shown to phosphorylate S383 and T649 in FOXO1, but it was suspected that additional AMPK phosphorylation sites might exist (30). Several AMPK phosphorylation motifs have been described (15,22,31,32) and central elements are 2-3 basic and/or hydrophobic residues at position 3-7 N-terminally together with one hydrophobic residue at position 3-4 C-terminally of the phosphorylated residue. Interestingly, S22 in the NTD of FOXO1 fulfills these criteria and was predicted by the PhosphoNET software (33) as a potential AMPK site.

To analyze if AMPK can phosphorylate S22 *in vitro*, we first performed a liquid chromatography mass spectrometry (LC-MS) measurement and identified one major and one minor phosphorylation site by the occurrence of a +80 Da and +160 Da peak. Subsequent peptide digestion and LC-MSMS suggested S22 as an AMPK phosphorylation site in the NTD of FOXO1 (Fig. S5).

To confirm phosphorylation of S22 by AMPK, we incubated NTDΔ as well as the full NTD with purified AMPK and evaluated the chemical shifts in time-resolved 2D $^{1}H/^{15}N$ HMQC NMR experiments. Within 2 h, a gradual disappearance of the S22 chemical shift at 8.36/116.64 ($^{1}H/^{15}N$) ppm was observed in combination with the emergence of two new peaks at 9.04/118.80 ($^{1}H/^{15}N$) ppm and 9.09/118.65 ($^{1}H/^{15}N$) ppm, indicating that S22 was phosphorylated by AMPK (Fig. 2A, Fig. S3A). Flanking residues next to the phosphorylation site were shifted in the NMR spectra (L17/27, R19/29, R21, C23, T24 and Y25) as observed for the phosphorylation of T24 by AKT within the same region. There was no substantial difference between the SSP scores of the unphosphorylated and S22 phosphorylated NTDΔ (Fig. S2). Hence, neither S22 nor T24 phosphorylation changed the secondary structure of this region of the NTD.

Phosphorylation of S22 by AMPK decreases phosphorylation of T24 by AKT

Downloaded from http://www.jbc.org/ by guest on January 9, 2020

The proximity of S22 and T24 led us explore if the phosphorylation status of one of those residues affects the subsequent phosphorylation of the other site or whether phosphorylation occurs independently. Time-resolved 2D NMR experiments on the pre-phosphorylated NTDΔ were conducted. NTDΔ-pT24 was incubated with purified AMPK and over the course of 4.5 h, two peaks assigned to S22 at 8.53/117.87 ($^{1}H/^{15}N$) ppm and 8.37/117.71 ($^{1}H/^{15}N$) ppm disappeared (Fig. 2B, shown in red). In parallel, two new peaks appeared at 9.07/119.49 ($^{1}H/^{15}N$) ppm and 9.11/119.14 ($^{1}H/^{15}N$) ppm, illustrating successful phosphorylation of S22. Full phosphorylation of S22 in NTDΔ-pT24 was achieved after about 4.5 h, approximately twice the time in comparison to the unphosphorylated protein as a substrate. Next, we incubated NTDΔ-pS22 with AKT. No peaks were shifted in the NMR spectra after 4.5 h, highlighting that AKT was unable to phosphorylate T24 within this time scale (Fig. 2B, shown in orange). After 24 h, a weak signal appeared for pT24 with a concomitant decrease in intensity of the T24 peak, suggesting a very weak phosphorylation by AKT (data not shown). Comparable results were observed with the full NTD (Fig. S3B). Taken together, the prior phosphorylation status of S22 drastically affected subsequent phosphorylation of T24 by AKT, but pT24 only moderately reduced the phosphorylation rate of S22 by AMPK.

To further substantiate this observation, Michaelis-Menten kinetics (K_M) were determined for AMPK and AKT with the unphosphorylated and pre-phosphorylated NTD. For AMPK, the K_M of the unphosphorylated NTD and NTD-pT24 as a substrate was 32 µM and 74 µM, respectively (Fig. 2C, right panel). This statistically significant ($p = 0.0016$) 2.3-fold increase of K_M was in a similar range as observed in the NMR measurements. For AKT, the K_M was 52 µM for the unphosphorylated NTD while the K_M could not be determined for the NTD-pS22, implying it is a poor AKT substrate (Fig. 2C, left panel).

Overall, time-resolved 2D NMR measurements combined with the biochemical assay demonstrate a hierarchical order, whereby the AMPK-mediated phosphorylation of S22 in the NTD has a strong regulatory effect on T24 phosphorylation by AKT but not *vice versa*.

Phosphorylation of S22 prevents interactions of FOXO1 with 14-3-3 proteins

A major mechanism to control FOXO1 transcriptional activity is the binding of 14-3-3 proteins. Different 14-3-3 interaction motifs have been described in the literature and FOXO1 contains two mode-I motifs, RXX(pS/pT)XP (34). A prerequisite for complex formation is the phosphorylation of one residue in each of the 14-3-3 interaction motifs by AKT; T24 and S256 (11). Interestingly, S22 is located in the N-terminal 14-3-3 binding interface (Fig. S8B). To examine the impact of S22 phosphorylation on 14-3-3 binding, we first studied the interaction of the NTD and 14-3-3 proteins *in vitro* using surface plasmon resonance (SPR) direct binding assays. 14-3-3 ζ was immobilized to the SPR sensor surface and binding affinities of the unphosphorylated NTD or the NTD phosphorylated on S22, T24 or both residues were measured. As expected, an AKT phosphorylated NTD (pT24) caused a strong interaction with 14-3-3 ζ (Kd 5.1 µM), confirming the central role of pT24 as binding platform for 14-3-3 proteins (Fig. 3A). An AMPK phosphorylated NTD (pS22) showed a very weak affinity to 14-3-3 ζ. Interestingly, the double phosphorylated NTD (pS22/pT24) also possessed a reduced affinity for 14-3-3 ζ of >50-fold (Kd 260 µM). Similar results were observed with the θ isoform of 14-3-3 (Fig. S6A) and it appeared that phosphorylation of S22 strongly blocked 14-3-3 binding even in the context of phosphorylated T24.

Crystal structures of pT24 and pS256 peptides in complex with 14-3-3 σ

To fully understand the consequence of S22 phosphorylation on 14-3-3 binding we aimed to crystallize the interface of the NTD and 14-3-3. However, no crystals could be obtained with the full NTD and therefore peptides were used to represent the different phosphorylated 14-3-3 recognition sites of FOXO1. The peptide representing the pT24 site consists of 11 amino acids with the sequence 18-RPRSCTWPLPR-30.

First, FAM-labelled versions of the peptides in different phosphorylation states were used in fluorescence anisotropy (FA) measurements to test, whether they reflect the binding behaviour

Downloaded from http://www.jbc.org/ by guest on January 9, 2020

between the NTD and 14-3-3 proteins observed in SPR experiments. The highest affinity was measured between 14-3-3 σ and the pT24 peptide (30 nM) while the pS22 and double phosphorylated peptides had weaker binding affinities (Fig. 3B). For 14-3-3 ζ, the pT24 peptide had an affinity of 18.3 nM whereas the double phosphorylated peptide had a binding affinity of 12.9 μM (Fig. S6B). Moreover, the binding of the pS22 and unphosphorylated peptide could not be quantified. Together, these results are in line with the findings of the SPR experiments employing the entire NTD.

Next, unlabeled peptides were used for structure analysis. The pT24 peptide in complex with 14-3-3 σ produced crystals of the space group $P2_1$ that diffracted to 2.3 Å and harbored eight 14-3-3/peptide molecules in the asymmetric unit (Fig. S7A). Up to nine residues out of the eleven amino acids comprising the pT24 peptide could be built into the electron density (Fig. 3C). The peptide binds into the amphipathic groove of the 14-3-3 protein, whereby the side-chain of W25 establishes an extensive hydrophobic contact with the "hydrophobic roof" (35) of the 14-3-3 monomer binding channel. The two prolines (P26 and P27) induce a strong turn in the peptide guiding the chain away from the W25 position towards the 14-3-3 dimer interface and out of the central binding channel. The pT24 is coordinated by K49, R57, R129, and Y130 of the protein. Additional polar contacts were mainly established via the peptide backbone and polar residues of 14-3-3 (carbonyl of W25 with K122, nitrogen of W25 with N175 and nitrogen of R21 with E182) (Fig. 3D). Interestingly, the hydroxyl group of S22 forms a polar contact with E182, locking this residue in all 8 monomers in a similar conformation (Fig. S7A). A close-up of that conformation explains how a phosphorylation of this residues disrupts the binding of the double phosphorylated peptide and the NTD: the serine fills a flat pocket of the 14-3-3 surface; any extension of that residue will cause a steric clash with the protein and therefore impair binding.

To complete the picture of FOXO1 binding to 14-3-3, the structure was also solved of the complex between pS256 and the C-terminal 14-3-3 binding site to 1.9 Å and in the space group $P2_12_12_1$, with two molecules found in the asymmetric unit (Fig. S7C). Seven residues (R252 – D258) out of the twelve amino acids comprising the FOXO1-pS256 peptide (251-RRRAASMDNNSK-262) could be built into the electron density (Fig. 3E). The phosphorylated serine (pS256) is found in the same pocket as the pT24, coordinated by R57, R129, and Y130 residues of 14-3-3 (Fig. 3F). The "hydrophobic roof" of the 14-3-3 monomer binding channel is occupied by the side-chain of M257, while residues D258 and N259 extend out of the binding groove. The small side-chain of the x-2 residue, A254, is in a similar position to the corresponding residue S22, however, it lacks the opportunity to engage in a polar contact with E182 in 14-3-3. These results emphasize a distinct feature of the N-terminal 14-3-3 binding site, where interactions can be directly regulated through phosphorylation of both T24 and S22.

S22 phosphorylation hinders 14-3-3 interactions in cells

To further investigate the significance of S22 and T24 phosphorylation regarding 14-3-3 interactions in a cellular context, we used FOXO1 (1-280) constructs (Fig. 1B) bearing either phosphodeficient (S22A and T24A) or phosphomimetic (S22E) mutations for immunoprecipitations in HEK293 cells. Amino acids 1-280 of FOXO1 contained both 14-3-3 interaction motifs, yet it was observed that a single point mutation (T24A) in the N-terminal binding site is sufficient to strongly reduce the overall 14-3-3 interactions due to loss of avidity (13). The wild-type construct was phosphorylated on T24 and precipitated, as expected, various isoforms of 14-3-3 proteins (Fig. 4A). Phosphorylation of T24 was a consequence of continuous AKT activity under optimal growth conditions confirmed with the pAKT antibodies (T308 and S473). For our experiments, we selected a HEK293 cell line with low endogenous FOXO1 levels and therefore we could ensure the signal of the pFOXO1 (T24) antibody represented the phosphorylation status of the ectopically expressed proteins. The T24A mutation that prevented phosphorylation by AKT, strongly reduced 14-3-3 interactions as previously described (13,36). The S22E mutation reflected an intracellular state of continuous AMPK activity, where S22 is phosphorylated, and strikingly showed an attenuated 14-3-3 binding

Downloaded from http://www.jbc.org/ by guest on January 9, 2020

comparable to the T24A mutation. The structural data proposed that mimicking the S22 phosphorylation directly prevents 14-3-3 binding through steric hindrance and electrostatic repulsion in the binding pocket. Moreover, despite active AKT, T24 phosphorylation was not detectable and it seemed that S22 phosphorylation additionally controls 14-3-3 binding indirectly through preventing AKT from accessing its phosphorylation site. This is consistent with our *in vitro* data that showed NTD-pS22 is a poor AKT substrate. Overall, our results substantiate the central role of the phosphorylation state of S22 to control binding of 14-3-3 proteins and thus regulating the transcriptional activity of FOXO1.

Discussion

FOXO transcription factors orchestrate the expression of genes involved in central cellular processes such as apoptosis, cell cycle progression and stress resistance. Among the plethora of post-translational modifications that regulate FOXO1 transcriptional activity, phosphorylation by AKT and the energy-sensing AMPK act in an opposing fashion. AKT-mediated phosphorylation of FOXO1 induces binding of 14-3-3 proteins, its nuclear export and consequent transcriptional inactivation (13), while phosphorylation by AMPK was shown to increase FOXO1 activity (37). In this work, we expand the interaction network of AKT and AMPK on FOXO1 by demonstrating that AMPK can phosphorylate the NTD of FOXO1 on S22 to affect 14-3-3 interactions.

An attenuated binding of 14-3-3 proteins to FOXO1, caused by phosphorylation of S22, could be explained by (i) conformational changes within the NTD of FOXO1, (ii) steric and electrostatic effects decreasing the binding affinity between FOXO1 and 14-3-3, or (iii) a reduction of AKT-mediated phosphorylation of T24 in FOXO1.

Conformational switching driven by post-translational modification of IDPs has been shown, for example, for Nucleophosmin (NPM1), where successive multiple phosphorylations induce a change from an ordered pentamer to a disordered monomeric state to control its function (30). Another example includes 4EBP2, where phosphorylation by ERK2 induces a conformational change from a disordered to a folded structure to form a regulatory switch (38). Our NMR results showed that no conformational changes occur in the NTD of FOXO1 by neither S22 nor T24 phosphorylation and thus exclude this as a probable cause to modulate 14-3-3 binding.

Another possibility could be that phosphorylation of S22 indirectly prevents 14-3-3 interactions by diminishing T24 phosphorylation by AKT. In a cellular context, we observed that AKT was unable to phosphorylate T24 in the phosphomimetic S22E FOXO1, whereas the phosphodeficient S22A as well as wild-type FOXO1 were unaffected. Moreover, time-resolved 2D NMR and measuring the Michaelis-Menten kinetics also showed that a pS22 impedes T24 phosphorylation by AKT. Interestingly, the crystal structure of AKT with bound substrate (39) suggests that a phospho-serine in the -2 position of the AKT phosphorylation site would be unfavorable electrostatically, leading to steric hindrance and hence obstructing binding of AKT. A similar sensitivity to mutations in the AKT binding motif was observed in patients with diffuse large B-cell lymphoma (DLBCL) (36). It was shown that the presence of point mutations at R19, R21 in the NTD of FOXO1 diminished phosphorylation of T24 by AKT, as we observed for pS22. Together, this emphasizes that phosphorylation of S22 renders the NTD a poor substrate for AKT and therefore diminishes T24 phosphorylation. This in turn will reduce 14-3-3 interactions and activate FOXO1.

Besides the effect on phosphorylation of T24 by AKT, we observed that phosphorylation of S22 directly reduces the affinity for the ζ and θ isoforms of 14-3-3 in SPR measurements. Our structure of 14-3-3 σ and a pT24 FOXO1 peptide further showed that phosphorylation of S22 at the -2 position of the canonically phosphorylated serine or threonine in the 14-3-3 motif would lead to both electrostatic repulsion and steric hindrance. Comparable alleviations of 14-3-3 binding through phosphorylation at the same position within the binding surface have previously been reported for RGS18 (40) and kinesin-14 (41). The effect of steric hindrance at the -2 position is additionally illustrated by a

Downloaded from http://www.jbc.org/ by guest on January 9, 2020

mutation in C-Raf, where a mutation of serine to a leucine (S257L) reduces 14-3-3 binding (42). Together, the phosphorylation status of S22 will translate into regulatory effects on 14-3-3 binding through steric and electrostatic forces in the binding pocket.

A sequence alignment of the human FOXO proteins shows full conservation of the serine corresponding to S22 in FOXO1 within the N-terminal 14-3-3 recognition motif (Fig. S8B). This offers the possibility that other FOXO family members might be subjected to a similar modulation of 14-3-3 binding through phosphorylation of the conserved serine. However, the kinases involved could vary between different FOXO family members due to sequence differences in the proximity of the phosphorylation site. AMPK is capable to recognize promiscuous substrates, yet a hydrophobic residue N-terminal of its phosphorylation site is a core feature in the recognition motif. Strikingly, this hydrophobic residue in position -7 (L17 in FOXO1) is only present in FOXO1, whereas FOXO3, 4 and 6 have a polar glutamine residue in the corresponding position that is likely to prevent AMPK binding (Fig. S8B). In fact, upon inhibition of AMPK, a decreased transcriptional activity of FOXO1 was observed, while the activity of FOXO3 was unaffected (19). Whether the AKT-mediated binding of 14-3-3 proteins can be modified through a crosstalk between diverse kinases in different FOXO proteins awaits further analysis. The key components of both PI3K/AKT and AMPK signaling pathways are well conserved throughout evolution. Interestingly, sequence alignments of different FOXO1 homologs between various species suggests that the additional regulation of 14-3-3 binding by AMPK might have evolved in vertebrates as indicated by a conserved AMPK recognition motif. In *D. melanogaster*, two residues of the AMPK recognition motif are substituted with amino acids that contain different chemical properties. This makes it unlikely that dFoxO is subjected to a comparable regulation by AMPK. Finally, the direct impairment of 14-3-3 binding through phosphorylation at the -2 position by specific kinases may be a general regulation mechanism among 14-3-3 substrates since a bioinformatic analysis revealed a serine as the most prevalent residue at this position (34).

AMPK and AKT pathways are heavily intertwined by negative feedback loops. This makes it challenging to quantify the specific contribution of the S22 phosphorylation regarding FOXO1 regulation in a cellular context. Furthermore, interpretation of data and literature is complicated as tool compounds used to influence AMPK activity (i.e. resveratrol and AICAR) can lead to secondary effects. Cell and tissue related differences in signaling pathways and particularly AMPK and AKT activity further hamper interpretation of the data. Even though AMPK and AKT act antagonistically on each other and FOXO1, cellular conditions have been described where both kinases are simultaneously active (43-45). In the latter publication, Zou et al. suggested that metformin activates FOXO1 via AMPK signaling through impeding phosphorylation by AKT and concomitantly increasing its nuclear localization. Although phosphorylation of FOXO1 was only analyzed on S256 and not T24 in that study, the mechanism where phosphorylation of S22 by AMPK leads to loss of 14-3-3 interactions could in part explain the described nuclear retention of FOXO1. Another report described enhanced FOXO1 transcriptional activity after H_2O_2 treatment, which is known to activate AMPK. Paradoxically, the increased transcriptional activity was accompanied by a higher level of AKT phosphorylated pFOXO1 (46). This could be a consequence of increased AMPK activity under these conditions that might overrule the AKT-mediated export of FOXO1 from the nucleus to the cytoplasm. Although further studies are required to fully understand the observed crosstalk between AMPK and AKT signaling to regulate FOXO1 activity as well as the relevant cellular context, we demonstrate a hierarchy in its kinase regulation. Thereby, AKT and AMPK pathways directly integrate on FOXO1 with the potential to fine-tune its transcriptional activity through interactions with 14-3-3 proteins.

Downloaded from http://www.jbc.org/ by guest on January 9, 2020

Experimental procedures

Vector construction

FOXO1 constructs were synthesized by GeneArt and codon optimized for expression in respective host cells. FOXO1 constructs (NTDΔ and NTD) contained a N-terminal 6xHN-tag as well as TEV protease cleavage site for purification of recombinant proteins and were cloned into a pET-24 vector. FOXO1 (1-280) constructs (wild-type, S22A, S22E, T24A) that were used in cell experiments carried an N-terminal 3xFLAG-tag as well as C-terminal EGFP and were cloned into a pcDNA3.1 vector.

Expression and purification of FOXO1 proteins

NTDΔ and NTD were expressed in *Escherichia coli* BL21 Star (DE3). TB media was supplemented with kanamycin (100 mg/l), 3 mM $MgCl_2$, 0.8% glycerol, 0.02% glucose and 0.2% lactose for auto-induction (47). The cells were grown at 37ºC for 4 h, followed by 20 h growth at 20ºC before lysis in HEPES buffer pH 7.4, 150 mM NaCl, 1 mM TCEP, 1x protease inhibitors (Roche #26733200) using a cell disruptor at 25 ksi (Constant Systems). The protein was captured on a HisTrap FF column (GE Healthcare) and subsequently eluted in increasing imidazole concentrations (10-400 mM). The protein was further purified on a size exclusion S75 column (GE Healthcare) that was pre-equilibrated in 20 mM Tris-HCl pH 7.4, 150 mM NaCl, 1 mM TCEP and 1x protease inhibitors.

The double isotopically labeled protein ($^{13}C/^{15}N$) was expressed in *Escherichia coli* BL21 Star (DE3) and grown in TB until an OD of 2. Then, cells were harvested by centrifugation at 4500 g for 5 min and resuspended in half the volume of Optimized High Cell Density Minimal Medium (48) supplemented with $^{15}NH_4Cl$ (Cambridge Isotope Lab, CIL #NLM-467-PK) and ^{13}C glucose (CIL #CLM-1396-PK). After 1 h adaptation at 37ºC, temperature was lowered to 20ºC and protein expression was induced with 0.5 mM IPTG for 16-48 h. Labelled proteins were purified as described above with exception of the final buffer that was for the NTD: 50 mM NaPi pH 6.8, 120 mM NaCl, 1 mM TCEP, 10% D_2O and for NTDΔ: 20 mM HEPES pH 6.7, 100 mM NaCl, 1 mM TCEP, 10% D_2O.

Peptides

EPLPRPRSCTWPLPRPE, EPLPRPR(pS)CTWPLPRPE (pS22) and EPLPRPRSC(pT)WPLPRPE (pT24) were purchased from Cambridge Research Biochemicals and diluted in H_2O. AKT1-PKB-α S473D (amino acids 118–480; in the text referred to as AKT) and 14-3-3 proteins (isoforms θ and ζ) were produced by the reagents and services division of the MRC protein phosphorylation and ubiquitylation unit of the University of Dundee [https://mrcppureagents.dundee.ac.uk] and stored at -80°C. AMPK (6xHis-α2; S108A-β2; γ1) was expressed and purified as previously described (18) and used at a stock concentration of 6 mg/ml in 120 mM Tris-HCl pH 8.0, 200 mM NaCl, 10% glycerol. The ADP biosensor 5-ATR-ParM (tetramethylrodamine labeled ParM protein) was expressed, purified and labeled as previously described (49).

Phosphorylation of FOXO1

The NTD of FOXO1 in 20 mM Tris-HCl pH 7.4, 150 mM NaCl, 1 mM TCEP, 1x protease inhibitor (Roche #26733200), and 0.1 mM Na_3VO_4 was supplemented with AKT or AMPK to a final concentration of 0.19 μM and 0.33 μM, respectively. For sequential phosphorylation of FOXO1, AKT was added overnight before the reaction could proceed with AMPK for one additional night at 20ºC. Prior to surface plasmon resonance experiments, the FOXO1 preparations were buffer exchanged to 10 mM HEPES pH 7.4, 350 mM NaCl, 1 mM TCEP and 0.05% v/v Tween 20 using a NAP-10 column. Samples were separated with Novex 4-12% Bis-Tris gels (Invitrogen) in 1x MES running buffer and phosphorylation was assessed by staining with Pro-Q Diamond Phosphoprotein Gel Stain (Invitrogen) followed by SYPRO Ruby Gel Stain (Invitrogen) and Phos-tag gels (Wako Pure Chemical Industries Ltd) stained with Instant Blue (Expedeon). Further confirmation of phosphorylation was performed by mass spectrometry, where the molecular mass of each FOXO1 sample was measured by MS-ESI micromass ZQ analysis (Waters). Samples were diluted in an equal volume of buffer A (0.1% formic acid, 3% acetonitrile) and separated over a C4 column (Dionex) in a chromatography from

Downloaded from http://www.jbc.org/ by guest on January 9, 2020

100% Buffer A to 100% Buffer B (0.1% formic acid, 90% acetonitrile). Mass spectroscopic data were analyzed with the MassLynx software.

Surface Plasmon Resonance

Experiments were performed on a Biacore 3000 (GE Healthcare) and either 14-3-3 θ or ζ were covalently immobilized on a low density CM5 chip (Xantec) using standard amine coupling procedures (EDC/NHS activation) with proteins in acetate buffer pH 5.5. The various FOXO1 preparations were injected at a concentration of 330 µM to 17 nM with 10-3 x dilution steps. The RU at steady state were recorded and data adjusted for non-specific binding observed with unphosphorylated FOXO1. Steady state data were fitted to a model with R_{max} fixed at 600 RU or 400 RU for 14-3-3 θ or ζ, respectively, using non-linear regression in Prism (GraphPad). Kinetic parameters K_{on} and K_{off} of the SPR raw data were extracted using curve fitting in the BiaEvaluation 4.1 software.

NMR

Measurements were recorded on an 800 MHz Bruker Avanze III spectrometer equipped with a cryogenic probe (Bruker) at 20°C with 330 µl sample in medium walled tubes. Spectral assignment was obtained by using 2D $^{1}H/^{15}N$ SOFAST HMQC and standard Bruker pulse sequence for triple resonance spectra 3D $^{1}H/^{15}N/^{13}C$ HNCαCβ, HNCα and HNCoCαCβ. All spectra were processed in TopSpin (Bruker) and CCPNMR (50) was used for sequential assignment of chemical shifts.

To follow the phosphorylation of the NTD by AKT or AMPK, a series of 2D $^{1}H/^{15}N$ SOFAST HMQC experiments were used for either 100 µM uniformly labelled $^{13}C/^{15}N$ NTD or 400 µM uniformly labelled $^{13}C/^{15}N$ NTDΔ. After complete phosphorylation, a 3D HNCαCβ spectra was recorded for assignment, followed by addition of the second kinase to obtain the other series of 2D $^{1}H/^{15}N$ SOFAST HMQC measurements. At completion of the phosphorylation, or after 24 h, a 3D HNCαCβ spectra was recorded for assignments of chemical shifts. $^{15}N/^{13}C$ Hα(Cα)N NMR spectra were recorded to assess conformation of prolines in the NTD and Hα/N peaks were identified.

The integrity of all proteins was monitored by SDS-PAGE after NMR analysis to assure no proteolytic cleavage occurred during the measurements.

NMR data deposition

BMRB codes: NTDΔ: 27336, NTDΔ-pS22: 27337, NTDΔ-pT24: 27320.

Secondary structure propensity analysis

The secondary chemical shifts (Δδ) were calculated as Δδ=δ–δrc where δ is the observed chemical shift and δrc is the random coil chemical shift (27,51). The presented SSP score is a weighted average of the Δδ shifts over five residues. Negative SSP values indicate a preference for β-strand or extended structure while positive values indicate an α-helical propensity. A weighted SSP score of 1 represents a full secondary structure. Prolines as well as residues preceding prolines were excluded in the analysis since prolines do not have the backbone amide proton. This makes them invisible in 2D $^{1}H/^{15}N$ HMQC and they strongly affect chemical shifts of flanking residues. The phosphorylated residues are not part of the reference database and hence, a correct comparison could not be made. These residues were excluded from the SSP analysis.

Biochemical enzymatic assay

The ADP sensing 5-ATR-ParM (tetramethylrodamine labeled ParM protein) (49) was used to measure kinase activities of AKT and AMPK. The assay was carried out in 30 mM Tris-HCl pH 7.5, 25 mM KCl, 10 mM $MgCl_2$ buffer, supplemented with fresh 1 mM TCEP, 5 µM BSA and 1 x protease inhibitors (Roche #26733200) at the day of experiment. FOXO1 peptides were dissolved in H_2O to a concentration of 20 mM. The assay was performed with a total assay volume of 12 µl in a Greiner microtiter plate (#784900). Under the assay conditions, the biosensor showed a linear response to ADP in the range of 1-400 µM ADP (Ultra-Pure, Promega). First, 0.05 µM 5-ATR-ParM, 1 mM ATP and varying concentrations of FOXO1 peptide (0.5 mM - 0.25 µM) were diluted in running buffer, centrifuged at 200 g for 1 min and incubated on ice. After 1 h, enzyme was added as well as AKT

Downloaded from http://www.jbc.org/ by guest on January 9, 2020

5 nM to 200 nM, for the NTD or NTD-pS22; or AMPK 5 nM to 25 nM, for the NTD or NTD-pT24. Substrates were pre-equilibrated. The plates were centrifuged at 200 g for 1 min, followed by kinetic measurements. The accumulation of ADP was assessed as increased fluorescent signal with an excitation at 540 nm and an emission filter at 590 nm using a PheraStar microplate reader (BMG Labtech). Data were recorded with an interval of 120 s for 1.5 h and analyzed with the MARS software (BMG Labtech). The initial linear velocity was extracted and plotted against substrate concentration in Prism (GraphPad). The initial velocity was normalized to the maximum initial velocity except for AKT with NTD-pS22. No activity could be measured and therefore data were scaled using normalization parameters from the measurement of AKT with the NTD. All experiments were performed in triplicates at least three separate times. Data were analyzed using a non-linear regression Michaelis-Menten model. A K_M for one run in a single experiment (AKT with the NTD; third out of four runs) was flagged as an outlier by a Grubb's outlier test and excluded from further analysis. Differences in K_M values were tested for significance with One-way ANOVA. The K_M shows a significant difference between AMPK with NTD and NTD-pT24 as substrates ($p = 0.0016$), the K_M differences are non-significant between AKT NTD and AMPK NTD or NTD-pT24 ($p = 0.0795$ and $p = 0{,}1592$, respectively). The K_M value couldn´t be determined for NTD-pS22 with AKT.

Crystallography

The 14-3-3σΔC protein (C-terminally truncated 14-3-3 σ, amino acids 1-231) was mixed in a 1:1 ratio each with either the FOXO1-pT24 or the FOXO1-pS256 peptide to a final concentration of 12 mg/mL of protein in buffer (20 mM HEPES pH 7.5, 2 mM $MgCl_2$, 2 mM BME). The 14-3-3σΔC/FOXO1-pT24 mixture was crystallized using the sitting drop method in a 1:1 ratio of 14-3-3σΔC/FOXO1-pT24 complex to crystallization buffer (0.1 M Bis-Tris propane, pH 7, 0.2 M sodium nitrate, 28% (v/v) PEG 400, 5% (w/v) glycerol) and incubated at 4°C. The 14-3-3σΔC/FOXO1-pS256 mixture was crystallized using the sitting drop method in a 1:1 ratio of 14-3-3σΔC/FOXO1-pS256 complex to crystallization buffer (0.1 M Bis-Tris propane, pH 7, 0.2 M sodium citrate tribasic dehydrate, 20% (w/v) PEG 3350, 10% (w/v) glycerol) and incubated at 4°C.

Diffraction data for the crystals were collected at the synchrotron (PETRA III, Hamburg) and processed with DIALS using xia2. The structures were solved by molecular replacement with a previously solved 14-3-3/peptide complex (PDB ID: 3MHR), using molrep for the 14-3-3σΔC/FOXO1-pT24 structure, and Phaser-MR for the 14-3-3σΔC/FOXO1-pS256 structure. Model building and refinement of both structures was performed using Coot, REFMAC5 and phenix.refine.

PDB accession number

14-3-3σΔC/FOXO1-pT24: 6QZR
14-3-3σΔC/FOXO1-pS256: 6QZS

Cell culture and plasmid DNA transfection

HEK293 cells were free of mycoplasma and authenticated by STR DNA profiling analysis. Cells were grown in DMEM (Gibco, #31966) supplemented with 10% FBS (Gibco, #10270-106) without antibiotics at 37°C in 5% CO_2. Plasmid DNA was transfected with FuGENE HD Transfection Reagent (Promega) according to the manufacturer´s protocol.

FLAG immunoprecipitation

Anti-FLAG M2-Agarose affinity gel (A2220) was purchased from Sigma-Aldrich and immunoprecipitations were performed according to the manufacturer's instructions. In brief, HEK293 cells were transfected in 10 cm dishes with 10 µg of FLAG-tagged fusion proteins. 20 h post transfection, cells were washed with ice-cold PBS and resuspended in 1 ml lysis buffer (20 mM Tris-HCl pH 7.4, 150 mM NaCl, 1% Triton X-100 (v/v), 2 mM EDTA, 25 mM NaF, 1 mM Na_3VO_4, 1x cOmplete protease inhibitor cocktail (Roche #26733200)). After incubation on ice for 20 min, lysates were sonicated and cleared by centrifugation (12000 g for 10 min) before cell extracts were incubated with anti-FLAG M2 beads for 90 min while rotating. Beads were washed with 20 mM Tris-HCl pH 7.4, 150 mM NaCl and protein complexes were eluted with

Downloaded from http://www.jbc.org/ by guest on January 9, 2020

SDS sample buffer (without DTT). DTT was added to 50 mM final concentration before SDS PAGE. All steps were performed at 4°C.

Western blotting and antibodies

Equal amounts of proteins were separated on 4-12% Bis-Tris gels (Invitrogen) in MES buffer and transferred to nitrocellulose membranes with a Trans-Blot Turbo system (Bio-Rad).

pFOXO1-T24 (#9464), pFOXO1-S256 (#9461), 14-3-3 (#8312), AKT (#2938), pAKT-S473 (#4060) and pAKT-T308 (#13038) antibodies were purchased from Cell Signaling Technology. β-Actin (A1978) and FLAG (F3165) antibodies from Sigma-Aldrich. IRDye secondary antibodies for Western blotting were from LI-COR and membranes were scanned using an Odyssey CLx imaging system (LI-COR).

Acknowledgements: We would like to thank Rachel Rowlinson, Anna Hoyle and Melanie Snow for help with LC-MSMS (Discovery Sciences, R&D, AstraZeneca, UK), Puneet Ahuja for NMR setup (Discovery Sciences, R&D, AstraZeneca, Sweden) Mats Ormö for support with the ADP biosensor assay (Discovery Sciences, R&D, AstraZeneca, Sweden) and Ryan Guillbert for providing the ParM protein (Discovery Sciences, R&D, AstraZeneca, UK). M.S. and T.J were, L.B. is a fellow of the AstraZeneca postdoc program.

Conflict of interest: L.B., A.G., T.N. and A.S. are employees and shareholders of AstraZeneca. T.J. is an employee and shareholder of Nuevolution. M.S., M.W., R.L. and C.O. declare that they have no conflicts of interest with the contents of this article.

The abbreviations used are: FOXO, forkhead box O; NTD, N-terminal domain; FHD, Forkhead box domain; TAD, transcription activation domain; IDP, intrinsically disordered protein; AMPK, AMP-activated protein kinase; PI3K/AKT, phosphoinositide 3-kinase/AKT; SSP, secondary structure propensity; SPR, surface plasmon resonance; FA, fluorescence anisotropy;

Downloaded from http://www.jbc.org/ by guest on January 9, 2020

References

1. Martins, R., Lithgow, G. J., and Link, W. (2016) Long live FOXO: unraveling the role of FOXO proteins in aging and longevity. Aging Cell 15, 196-207

2. Hosaka, T., Biggs, W. H., 3rd, Tieu, D., Boyer, A. D., Varki, N. M., Cavenee, W. K., and Arden, K. C. (2004) Disruption of forkhead transcription factor (FOXO) family members in mice reveals their functional diversification. Proceedings of the National Academy of Sciences of the United States of America 101, 2975-2980

3. Klotz, L. O., Sanchez-Ramos, C., Prieto-Arroyo, I., Urbanek, P., Steinbrenner, H., and Monsalve, M. (2015) Redox regulation of FoxO transcription factors. Redox biology 6, 51-72

4. Zhao, Y., Wang, Y., and Zhu, W. G. (2011) Applications of post-translational modifications of FoxO family proteins in biological functions. Journal of molecular cell biology 3, 276-282

5. Rena, G., Guo, S., Cichy, S. C., Unterman, T. G., and Cohen, P. (1999) Phosphorylation of the transcription factor forkhead family member FKHR by protein kinase B. The Journal of biological chemistry 274, 17179-17183

6. Zhou, J., Li, H., Li, X., Zhang, G., Niu, Y., Yuan, Z., Herrup, K., Zhang, Y. W., Bu, G., Xu, H., and Zhang, J. (2015) The roles of Cdk5-mediated subcellular localization of FOXO1 in neuronal death. J Neurosci 35, 2624-2635

7. Lee, J. W., Chen, H., Pullikotil, P., and Quon, M. J. (2011) Protein kinase A-alpha directly phosphorylates FoxO1 in vascular endothelial cells to regulate expression of vascular cellular adhesion molecule-1 mRNA. The Journal of biological chemistry 286, 6423-6432

8. Huang, H., Regan, K. M., Lou, Z., Chen, J., and Tindall, D. J. (2006) CDK2-dependent phosphorylation of FOXO1 as an apoptotic response to DNA damage. Science (New York, N.Y.) 314, 294-297

9. Yuan, Z., Becker, E. B., Merlo, P., Yamada, T., DiBacco, S., Konishi, Y., Schaefer, E. M., and Bonni, A. (2008) Activation of FOXO1 by Cdk1 in cycling cells and postmitotic neurons. Science (New York, N.Y.) 319, 1665-1668

10. Rena, G., Woods, Y. L., Prescott, A. R., Peggie, M., Unterman, T. G., Williams, M. R., and Cohen, P. (2002) Two novel phosphorylation sites on FKHR that are critical for its nuclear exclusion. The EMBO journal 21, 2263-2271

11. Brunet, A., Bonni, A., Zigmond, M. J., Lin, M. Z., Juo, P., Hu, L. S., Anderson, M. J., Arden, K. C., Blenis, J., and Greenberg, M. E. (1999) Akt promotes cell survival by phosphorylating and inhibiting a Forkhead transcription factor. Cell 96, 857-868

12. Tang, E. D., Nunez, G., Barr, F. G., and Guan, K. L. (1999) Negative regulation of the forkhead transcription factor FKHR by Akt. The Journal of biological chemistry 274, 16741-16746

13. Rena, G., Prescott, A. R., Guo, S., Cohen, P., and Unterman, T. G. (2001) Roles of the forkhead in rhabdomyosarcoma (FKHR) phosphorylation sites in regulating 14-3-3 binding, transactivation and nuclear targetting. Biochemical Journal 354, 605-612

14. Matsuzaki, H., Daitoku, H., Hatta, M., Tanaka, K., and Fukamizu, A. (2003) Insulin-induced phosphorylation of FKHR (Foxo1) targets to proteasomal degradation. Proceedings of the National Academy of Sciences of the United States of America 100, 11285-11290

Downloaded from http://www.jbc.org/ by guest on January 9, 2020

15. Yun, H., Park, S., Kim, M. J., Yang, W. K., Im, D. U., Yang, K. R., Hong, J., Choe, W., Kang, I., Kim, S. S., and Ha, J. (2014) AMP-activated protein kinase mediates the antioxidant effects of resveratrol through regulation of the transcription factor FoxO1. The FEBS journal 281, 4421-4438

16. Yuan, Z., Lehtinen, M. K., Merlo, P., Villén, J., Gygi, S., and Bonni, A. (2009) Regulation of Neuronal Cell Death by MST1-FOXO1 Signaling. The Journal of biological chemistry 284, 11285-11292

17. Asada, S., Daitoku, H., Matsuzaki, H., Saito, T., Sudo, T., Mukai, H., Iwashita, S., Kako, K., Kishi, T., Kasuya, Y., and Fukamizu, A. (2007) Mitogen-activated protein kinases, Erk and p38, phosphorylate and regulate Foxo1. Cellular signalling 19, 519-527

18. Xiao, B., Sanders, M. J., Carmena, D., Bright, N. J., Haire, L. F., Underwood, E., Patel, B. R., Heath, R. B., Walker, P. A., Hallen, S., Giordanetto, F., Martin, S. R., Carling, D., and Gamblin, S. J. (2013) Structural basis of AMPK regulation by small molecule activators. Nature communications 4, 3017

19. Awad, H., Nolette, N., Hinton, M., and Dakshinamurti, S. (2014) AMPK and FoxO1 regulate catalase expression in hypoxic pulmonary arterial smooth muscle. Pediatric pulmonology 49, 885-897

20. Chen, B. L., Ma, Y. D., Meng, R. S., Xiong, Z. J., Wang, H. N., Zeng, J. Y., Liu, C., and Dong, Y. G. (2010) Activation of AMPK inhibits cardiomyocyte hypertrophy by modulating of the FOXO1/MuRF1 signaling pathway in vitro. Acta pharmacologica Sinica 31, 798-804

21. Lee, K., Ochi, E., Song, H., and Nakazato, K. (2015) Activation of AMP-activated protein kinase induce expression of FoxO1, FoxO3a, and myostatin after exercise-induced muscle damage. Biochemical and biophysical research communications 466, 289-294

22. Greer, E. L., Dowlatshahi, D., Banko, M. R., Villen, J., Hoang, K., Blanchard, D., Gygi, S. P., and Brunet, A. (2007) An AMPK-FOXO pathway mediates longevity induced by a novel method of dietary restriction in C. elegans. Current biology: CB 17, 1646-1656

23. Xue, B., Dunbrack, R. L., Williams, R. W., Dunker, A. K., and Uversky, V. N. (2010) PONDR-FIT: a meta-predictor of intrinsically disordered amino acids. Biochimica et biophysica acta 1804, 996-1010

24. Obradovic, Z., Peng, K., Vucetic, S., Radivojac, P., Brown, C. J., and Dunker, A. K. (2003) Predicting intrinsic disorder from amino acid sequence. Proteins 53 Suppl 6, 566-572

25. Brent, M. M., Anand, R., and Marmorstein, R. (2008) Structural basis for DNA recognition by FoxO1 and its regulation by posttranslational modification. Structure 16, 1407-1416

26. Singh, P., Han, E. H., Endrizzi, J. A., O'Brien, R. M., and Chi, Y.-I. (2017) Crystal structures reveal a new and novel FoxO1 binding site within the human glucose-6-phosphatase catalytic subunit 1 gene promoter. Journal of Structural Biology 198, 54-64

27. Marsh, J. A., Singh, V. K., Jia, Z., and Forman-Kay, J. D. (2006) Sensitivity of secondary structure propensities to sequence differences between alpha- and gamma-synuclein: implications for fibrillation. Protein science: a publication of the Protein Society 15, 2795-2804

28. Selenko, P., Frueh, D. P., Elsaesser, S. J., Haas, W., Gygi, S. P., and Wagner, G. (2008) In situ observation of protein phosphorylation by high-resolution NMR spectroscopy. Nature structural & molecular biology 15, 321-329

Downloaded from http://www.jbc.org/ by guest on January 9, 2020

29. Reimer, U., and Fischer, G. (2002) Local structural changes caused by peptidyl-prolyl cis/trans isomerization in the native state of proteins. Biophysical chemistry 96, 203-212

30. Mitrea, D. M., Grace, C. R., Buljan, M., Yun, M.-K., Pytel, N. J., Satumba, J., Nourse, A., Park, C.-G., Madan Babu, M., White, S. W., and Kriwacki, R. W. (2014) Structural polymorphism in the N-terminal oligomerization domain of NPM1. Proceedings of the National Academy of Sciences 111, 4466-4471

31. Hardie, D. G. (2011) AMP-activated protein kinase: an energy sensor that regulates all aspects of cell function. Genes & development 25, 1895-1908

32. Marin, T. L., Gongol, B., Martin, M., King, S. J., Smith, L., Johnson, D. A., Subramaniam, S., Chien, S., and Shyy, J. Y. J. (2015) Identification of AMP-activated protein kinase targets by a consensus sequence search of the proteome. BMC Systems Biology 9, 13

33. Safaei, J., Manuch, J., Gupta, A., Stacho, L., and Pelech, S. (2011) Prediction of 492 human protein kinase substrate specificities. Proteome science 9 Suppl 1, S6

34. Johnson, C., Crowther, S., Stafford, Margaret J., Campbell, David G., Toth, R., and MacKintosh, C. (2010) Bioinformatic and experimental survey of 14-3-3-binding sites. Biochemical Journal 427, 69-78

35. Würtele, M., Jelich-Ottmann, C., Wittinghofer, A., and Oecking, C. (2003) Structural view of a fungal toxin acting on a 14-3-3 regulatory complex. The EMBO journal 22, 987-994

36. Trinh, D. L., Scott, D. W., Morin, R. D., Mendez-Lago, M., An, J., Jones, S. J., Mungall, A. J., Zhao, Y., Schein, J., Steidl, C., Connors, J. M., Gascoyne, R. D., and Marra, M. A. (2013) Analysis of FOXO1 mutations in diffuse large B-cell lymphoma. Blood 121, 3666-3674

37. Greer, E. L., Banko, M. R., and Brunet, A. (2009) AMP-activated Protein Kinase and FoxO Transcription Factors in Dietary Restriction–induced Longevity. Annals of the New York Academy of Sciences 1170, 688

38. Bah, A., Vernon, R. M., Siddiqui, Z., Krzeminski, M., Muhandiram, R., Zhao, C., Sonenberg, N., Kay, L. E., and Forman-Kay, J. D. (2015) Folding of an intrinsically disordered protein by phosphorylation as a regulatory switch. Nature 519, 106-109

39. Yang, J., Cron, P., Good, V. M., Thompson, V., Hemmings, B. A., and Barford, D. (2002) Crystal structure of an activated Akt/protein kinase B ternary complex with GSK3-peptide and AMP-PNP. Nature structural biology 9, 940-944

40. Gegenbauer, K., Elia, G., Blanco-Fernandez, A., and Smolenski, A. (2012) Regulator of G-protein signaling 18 integrates activating and inhibitory signaling in platelets. Blood 119, 3799-3807

41. Beaven, R., Bastos, R. N., Spanos, C., Rome, P., Cullen, C. F., Rappsilber, J., Giet, R., Goshima, G., and Ohkura, H. (2017) 14-3-3 regulation of Ncd reveals a new mechanism for targeting proteins to the spindle in oocytes. The Journal of cell biology 216, 3029-3039

42. Molzan, M., Schumacher, B., Ottmann, C., Baljuls, A., Polzien, L., Weyand, M., Thiel, P., Rose, R., Rose, M., Kuhenne, P., Kaiser, M., Rapp, U. R., Kuhlmann, J., and Ottmann, C. (2010) Impaired binding of 14-3-3 to C-RAF in Noonan syndrome suggests new approaches in diseases with increased Ras signaling. Molecular and cellular biology 30, 4698-4711

43. Pezze, P. D., Ruf, S., Sonntag, A. G., Langelaar-Makkinje, M., Hall, P., Heberle, A. M., Navas, P. R., van Eunen, K., Tölle, R. C., Schwarz, J. J., Wiese, H., Warscheid, B., Deitersen, J., Stork, B., Fäßler, E., Schäuble, S., Hahn, U., Horvatovich, P., Shanley, D. P., and Thedieck, K. (2016) A

Downloaded from http://www.jbc.org/ by guest on January 9, 2020

systems study reveals concurrent activation of AMPK and mTOR by amino acids. Nature communications 7, 13254

44. Leclerc, G. M., Leclerc, G. J., Fu, G., and Barredo, J. C. (2010) AMPK-induced activation of Akt by AICAR is mediated by IGF-1R dependent and independent mechanisms in acute lymphoblastic leukemia. Journal of Molecular Signaling 5, 15-15

45. Zou, J., Hong, L., Luo, C., Li, Z., Zhu, Y., Huang, T., Zhang, Y., Yuan, H., Hu, Y., Wen, T., Zhuang, W., Cai, B., Zhang, X., Huang, J., and Cheng, J. (2016) Metformin inhibits estrogen-dependent endometrial cancer cell growth by activating the AMPK–FOXO1 signal pathway. Cancer Science 107, 1806-1817

46. Ning, Y., Li, Z., and Qiu, Z. (2015) FOXO1 silence aggravates oxidative stress-promoted apoptosis in cardiomyocytes by reducing autophagy. The Journal of toxicological sciences 40, 637-645

47. Studier, F. W. (2005) Protein production by auto-induction in high density shaking cultures. Protein expression and purification 41, 207-234

48. Sivashanmugam, A., Murray, V., Cui, C., Zhang, Y., Wang, J., and Li, Q. (2009) Practical protocols for production of very high yields of recombinant proteins using Escherichia coli. Protein science: a publication of the Protein Society 18, 936-948

49. Kunzelmann, S., and Webb, M. R. (2010) A Fluorescent, Reagentless Biosensor for ADP Based on Tetramethylrhodamine-Labeled ParM. ACS Chemical Biology 5, 415-425

50. Vranken, W. F., Boucher, W., Stevens, T. J., Fogh, R. H., Pajon, A., Llinas, M., Ulrich, E. L., Markley, J. L., Ionides, J., and Laue, E. D. (2005) The CCPN data model for NMR spectroscopy: development of a software pipeline. Proteins 59, 687-696

51. Rosenlow, J., Isaksson, L., Mayzel, M., Lengqvist, J., and Orekhov, V. Y. (2014) Tyrosine phosphorylation within the intrinsically disordered cytosolic domains of the B-cell receptor: an NMR-based structural analysis. PloS one 9, e96199

Downloaded from http://www.jbc.org/ by guest on January 9, 2020

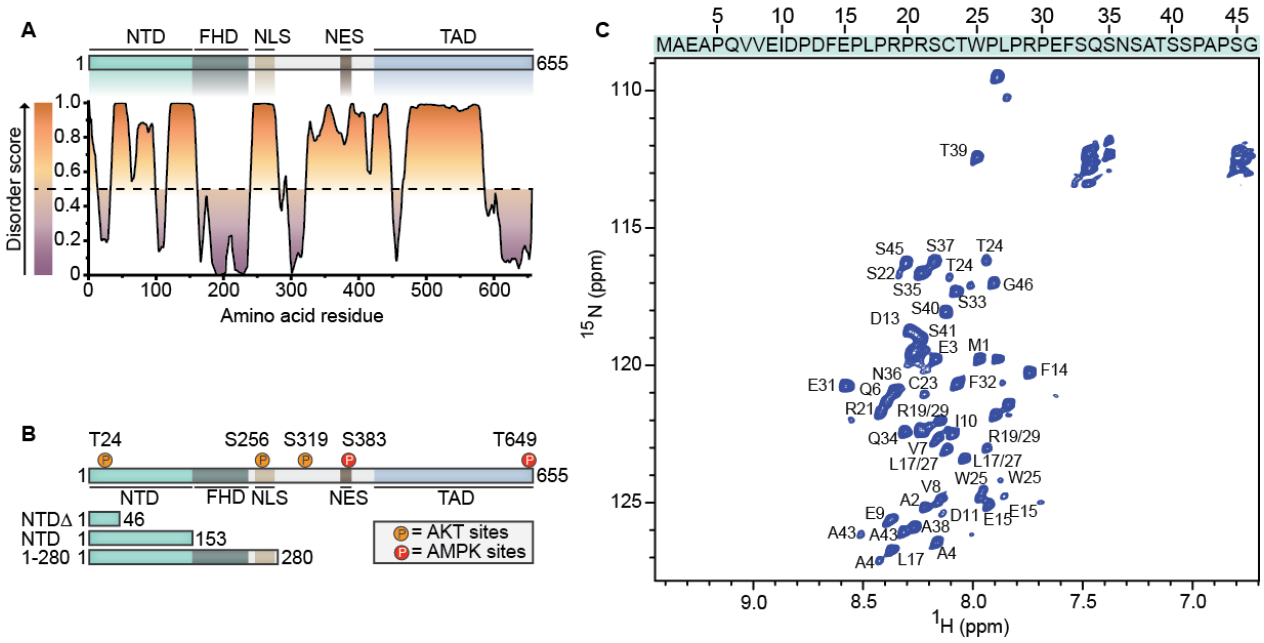

Figure 1. Analysis of intrinsically disordered regions in FOXO1 (A) Representation of the functional domains of FOXO1: NTD 1-153, FHD 154-244, TAD 421-655. A disorder score was predicted for each amino acid using PONDR-FIT. The dashed line at 0.5 of the Y-axis separates residues that were predicted disorderd (a score > 0.5, shown in orange) and ordered (a score < 0.5, shown in purple). **(B)** The known AKT and AMPK phosphorylation sites in FOXO1 are highlighted in orange and red, respectively. Constructs that have been used in this study are indicated: NTDΔ (1-46), NTD (1-153) and a fragment containing the NTD, FHD and NLS (1-280), which was used to analyze interactions with 14-3-3 proteins in cells (Figure 4A). **(C)** Assignment of the $^{1}H/^{15}N$ HMQC spectrum of NTDΔ. Several amino acids display pairs of signals, as these are preceded by prolines that occur in both *cis* and *trans* conformation. Amino acids L17/L27 and R19/R29 could not be distinguished since they are flanked by prolines, which do not show signals in a $^{1}H/^{15}N$ HMQC spectrum. Residues of the purification tag were observed but have not been assigned. Amino acids are indicated in one letter code.

Downloaded from http://www.jbc.org/ by guest on January 9, 2020

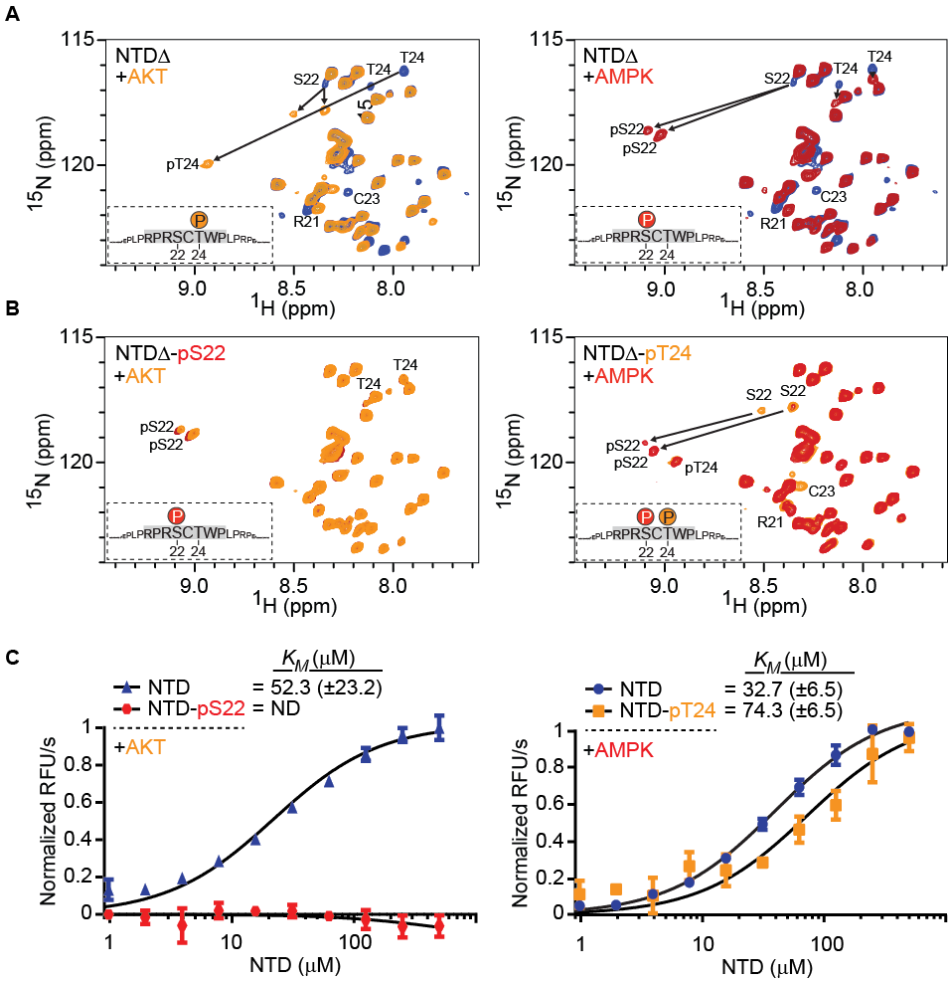

Figure 2. Phosphorylation of the NTD by AKT and AMPK (A) 2D $^{1}H/^{15}N$ HMQC NMR spectra of NTDΔ incubated for 3 h with purified AKT (in orange) or AMPK (in red) to assess T24 and S22 phosphorylation by AKT and AMPK, respectively. Chemical shift changes of phosphorylated amino acids are indicated by arrows. Doubling of peaks for pS22 suggest dual conformations. **(B)** 2D $^{1}H/^{15}N$ HMQC NMR spectra of pre-phosphorylated NTDΔ incubated with the indicated kinases for 4.5 h. NTDΔ-pS22 with AKT to monitor T24 phosphorylation (in orange) and NTDΔ-pT24 with AMPK to analyze S22 phosphorylation (in red). Chemical shift changes of phosphorylated amino acids are indicated by arrows. **(C)** The activities of both AKT and AMPK kinases on different substrates were analyzed using a fluorescence-based ADP biosensor. The unphosphorylated NTD as substrate for AKT and AMPK is shown in blue. The activity of AKT on NTD-pS22 is shown in red. The activity of AMPK on NTD-pT24 is shown in orange. Michaelis-Menten kinetics (K_M) were determined based on the initial reaction rates. Data are mean ± SD from three independent experiments. ND = Not detectable.

Downloaded from http://www.jbc.org/ by guest on January 9, 2020

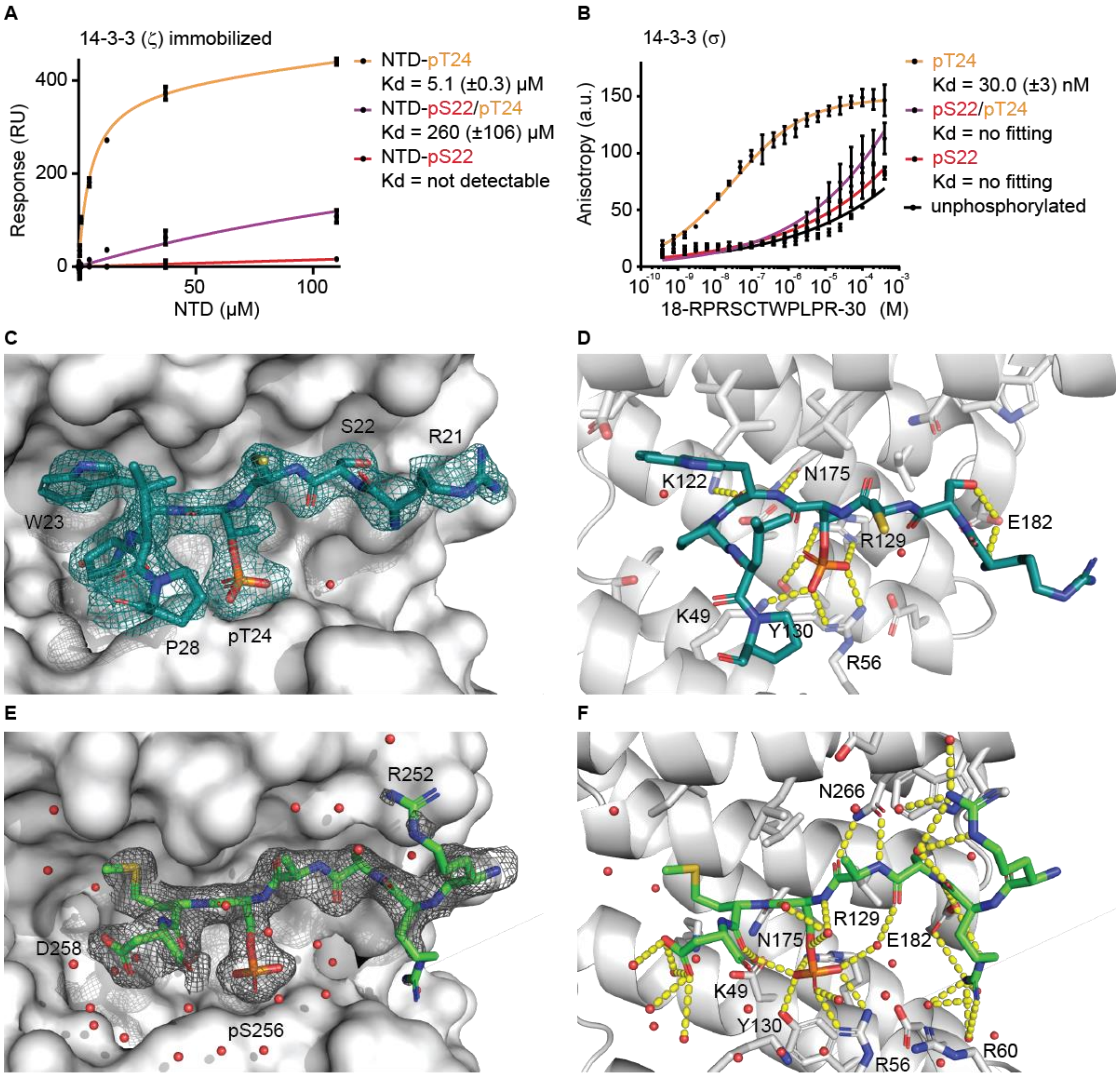

Figure 3. Phosphorylation of S22 in the NTD of FOXO1 hinders 14-3-3 interactions *in vitro* (A) Surface plasmon resonance binding analysis of 14-3-3 ζ and the NTD of FOXO1 phosphorylated at the indicated residues. NTD-pT24 served as positive control and the unphosphorylated NTD was used as linear component for data correction. Data are expressed as mean ± SD of technical triplicates from one representative experiment. **(B)** Fluorescence Anisotropy binding analysis of interactions between 14-3-3 σ and the FOXO1 peptide (18-RPRSCTWPLPR-30) in different phosphorylation states. Data are expressed as means ± SD from three independent experiments and fitted with Prism (Specific binding with Hill slope). **(C)** Representative FOXO1/14-3-3 complex with displayed electron density (Final 2Fo-Fc, contoured at 1σ) with 14-3-3 as grey surface, FOXO1-pT24 as sticks and water as red sphere. Amino acids of the FOXO1-pT24 peptide are indicated in one letter code. **(D)** Details of the interactions between FOXO1-pT24 and 14-3-3 σ. Amino acids of 14-3-3 σ are indicated in one letter code and hydrogen bonds are illustrated by yellow dashed lines. **(E)** FOXO1-pS256/14-3-3 complex with displayed electron density (Final 2Fo-Fc, contoured at 1σ) with 14-3-3 as grey surface, FOXO1-pS256 as sticks and water as red sphere. Amino acids of the FOXO1-pS256 peptide are indicated in one letter code. **(F)** Details of the interactions between FOXO1-pS256 and 14-3-3 σ. Amino acids of 14-3-3 σ are indicated in one letter code and hydrogen bonds are illustrated by yellow dashed lines.

Downloaded from http://www.jbc.org/ by guest on January 9, 2020

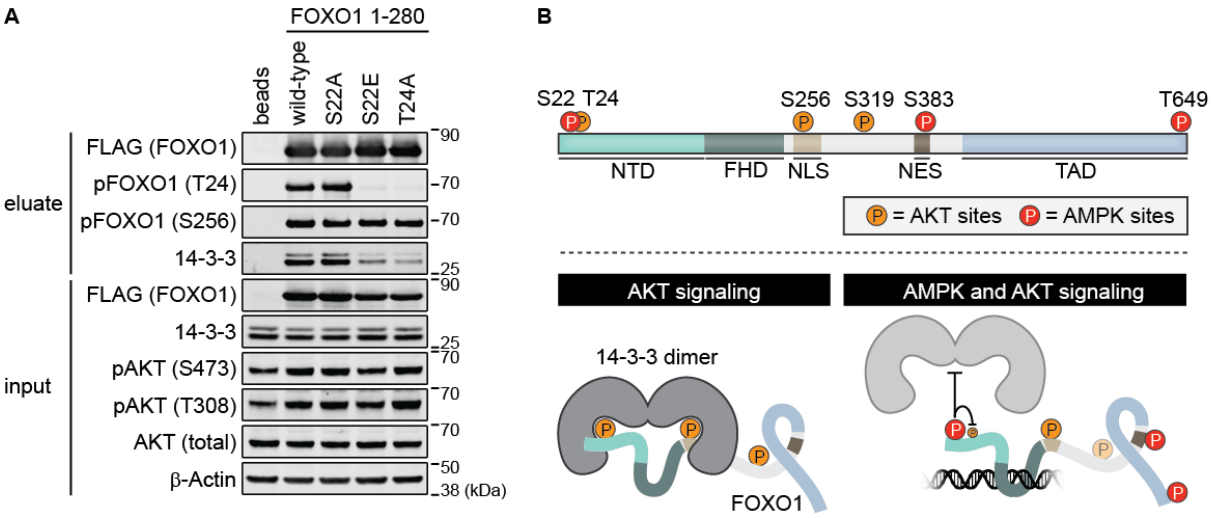

Figure 4. The phosphorylation state of S22 regulates binding of 14-3-3 proteins to FOXO1 in HEK293 cells (A) FLAG-FOXO1(1-280)-EGFP fusion proteins were expressed in HEK293 cells for 20 h. After cell lysis, complexes were immunoprecipitated using anti-FLAG agarose beads and analyzed by Western blotting with the indicated antibodies. Eluates were adjusted according to amounts of bait proteins (anti-FLAG). The T24A construct served as positive control for a reduced 14-3-3 interaction. The activity of AKT kinase was monitored with pAKT (S473/T308) antibodies. **(B)** Schematic overview of the regulation of transcriptional activity of FOXO1 by AKT and AMPK signaling pathways. Optimal growth conditions result in active AKT and phosphorylation of T24 as well as S256 in FOXO1 stimulates binding of 14-3-3 proteins to inhibit its transcriptional activity. On the other hand, phosphorylation of S22 by AMPK is likely to increase the activity of FOXO1 by preventing 14-3-3 binding both directly through steric hindrance and electrostatic repulsion and indirectly by attenuating T24 phosphorylation by AKT.

Downloaded from http://www.jbc.org/ by guest on January 9, 2020

AMPK and AKT protein kinases hierarchically phosphorylate the N-terminus of the FOXO1 transcription factor, modulating interactions with 14-3-3 proteins

Maria Saline, Lukas Badertscher, Madita Wolter, Roxanne Lau, Anders Gunnarsson, Tomas Jacso, Tyrrell Norris, Christian Ottmann and Arjan Snijder

J. Biol. Chem. published online July 15, 2019

Access the most updated version of this article at doi: 10.1074/jbc.RA119.008649

Alerts:
- When this article is cited
- When a correction for this article is posted

Click here to choose from all of JBC's e-mail alerts

Downloaded from http://www.jbc.org/ by guest on January 9, 2020

View publication stats